CrossMark

INVITED PAPER

Mechanical stresses at the cathode–electrolyte interface in lithium-ion batteries

Sangwook Kim and Hsiao-Ying Shadow Huang[a)]
Mechanical and Aerospace Engineering Department, North Carolina State University, Raleigh, NC 27695

(Received 31 May 2016; accepted 16 September 2016)

Experimental studies have shown capacity loss and impedance rise on the surfaces of cathode particles during (dis)charging in lithium-ion batteries. However, there are surprisingly few studies focusing on the cathode–electrolyte interface. The current study uses multiphysics finite element models to understand fluid–structure interactions in a half-cell battery system. Effects of C-rate, particle sizes, lithiation, and phase transformation of the cathode at the interface are investigated. Results demonstrate that doubling the particle size results in larger available lithium intercalation areas, giving rise to increased tension 1.40 times and compression 1.82 times at the interface. Moreover, higher C-rate with high lithium-ion concentration gradient results in higher mechanical stresses at the interface. These coupling factors are strongly related to the experimentally observed battery degradation. Our simulations demonstrate that both electrode and electrolyte have pronounced effects when investigating mechanical stresses at the electrode–electrolyte interface.

I. INTRODUCTION

Improving the performance and reliability of electrochemical energy storage systems such as lithium-ion batteries has the potential to enable emerging technologies such as wearable electronics and mechanized prosthetics for the disabled, as well as the successful integration of renewable energy by providing high capacity storage, leading to the expansion of market share for HEVs/EVs. Fast current-rates (C-rates) are considered essential for providing the high power and energy densities demanded by these new technologies.[1] However, it has been suggested that high C-rates play an important role in the mechanical and structural deterioration of lithium-insertion materials,[1] thereby progressively reducing the capacity of lithium-ion batteries with each charge/discharge cycle (referred to as "rate-capacity fade").[2] More than 25,000 studies have reported on anode (germanium, silicon, graphite/graphene, or carbon nanotube) and cathode materials ($LiCoO_2$, $LiMn_2O_4$, or $LiFePO_4$), and over 2000 studies have investigated the reduction of the electrolyte, leading to the formation of a solid–electrolyte interface at anode surfaces. However, there are far fewer studies on the cathode–electrolyte interface in lithium-ion batteries. Within these studies, chemical engineers, material scientists, and electrochemists have reported their findings in electrochemical reactions (i.e., electrolyte oxidation and cathode reduction), material stability, and associated kinetics. Yet, our basic knowledge of how mechanical stress states at the cathode–electrolyte interface contribute to battery performance and stability is currently extremely limited, hindering electrode and electrolyte materials innovation and the ability to use lithium-ion batteries as energy storage systems.

For example, Aurbach et al.[3,4] have studied the effects of acidic and nonacidic electrolytes on carbon-coated cathodes of $LiFePO_4$ during storage in different temperature, and the loss of active mass (i.e., Fe-ion dissolution) from the electrode was measured and indicates that the cathode was deteriorated by acidic electrolyte and high temperature. The experimental results from Ju et al.[5] suggest that the charge exchange process could take place at the interface between the cathode and electrolyte at the end of discharging after only five cycles. Strobridge et al.[6] used x-ray diffraction to map the evolution of the inhomogeneous electrochemical reaction in electrodes. Their results also show that a poorer electronic connection could result from both the expansion and the contraction of the cathode particles during cycling.[6] These observations suggest that electrolyte–electrode interactions and electrochemical reaction-induced volume changes in cathode materials ought to be studied as a whole.

Capacity fade is one of the most significant problems in lithium-ion batteries and can be associated with diffusion-induced stresses,[7–15] which have been studied in many electrode materials such as $LiCoO_2$, $LiMn_2O_4$, $LiFePO_4$, graphite,[16–23] etc. Specifically, these studies have focused on the effect of mechanical stress in lithium-ion batteries,[10–20,22–26] material structural characterization, and synthesis.[27–30] However, these studies

Contributing Editor: Yang-T. Cheng
[a)]Address all correspondence to this author.
e-mail: hshuang@ncsu.edu
DOI: 10.1557/jmr.2016.373

Downloaded from https://www.cambridge.org/core. North Carolina State University Libraries, on 05 Oct 2017 at 13:19:52, subject to the Cambridge Core terms of use, available at https://www.cambridge.org/core/terms. https://doi.org/10.1557/jmr.2016.373

generally emphasize only one component of the battery cells (i.e., either the cathode, anode or electrolyte). To better understand electrochemical and mechanical relationships in lithium-ion batteries, factors such as electrode particle sizes, electrolyte material, lithiation of the battery system, C-rate, and C-rate dependent volume change ought to be considered as a whole. It has been reported that concentration-dependent stiffening of anode materials (e.g., graphite) is beneficial for avoiding surface cracking.[15] ChiuHuang and Huang have previously reported less shear stress variability across the *bc*-plane of the cathode material when incorporating more realistic concentration-dependent material properties.[8,31] As such, concentration-dependent anisotropic material properties for the cathode and the associated phase transformation ought to be considered.

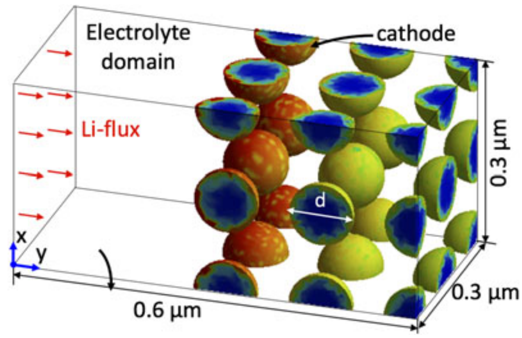

FIG. 1. Geometry of finite element model composed of two domains: electrolyte and electrode and symmetric boundary conditions are used. The half-cell system is modeled as a rectangular domain in which the electrolyte and spherical particles of cathode materials are included. One dimensional lithium-ion mass flux (J) along the y-axis is used as the driving force for the system.

II. METHOD

In this study, a computational model integrating experimental results[32] and theoretical analysis[33] is developed through a multiphysics analysis. Multiphysics finite element models for a half-cell system (i.e., with electrolyte and cathode) are developed using ANSYS Multiphysics (ANSYS, Inc., Canonsburg, Pennsylvania, USA). To adopt the concept of lithiation, a thermal stress analysis approach is used due to the similarity of the partial differential equations of Fourier's law for thermal conduction and Fick's law of diffusion.[8,19,20,34] In this study, due to the similarity of the partial differential equations of Fourier's law for thermal conduction and Fick's law of diffusion, the flux of lithium ions (J) is expressed as heat flux, and the temperature gradient represents the lithium-ion concentration gradient. Since the concepts of heat conduction and temperature are used for ionic diffusion and the concentration of lithium ion, effects of temperature and heat on the half-cell system are disregarded. The half-cell system is modeled as a $0.3 \times 0.3 \times 0.6$ μm rectangular domain in which the electrolyte and spherical particles of cathode materials are included (Fig. 1). The domain size is designed to resemble 300 nm thick $LiFePO_4$ films developed by Sauvage et al.[35] Thus, the long edge of the simulation domain will be set to $L = 0.6$ μm. After the convergence testing, 57,456 elements with the 10-node tetrahedral (T10) element type are used for cathode particles. Particles are modeled as spheres with rotational and translational degrees of freedom, and symmetric boundary conditions and fluid–solid interface boundary conditions are adopted. Four differently sized spherical particles[36,37] are included to investigate the effect of particle sizes (i.e., volume fraction). The associated volume fraction is calculated by dividing the volume of particles by the total volume of electrode domain. Thus, the models with 60, 80, 100, and 120 nm-sized particles have volume fractions of 3.3%, 8.0%, 15.5%, and 26.8%, respectively. C-rates are described by different lithium-ion fluxes (J), and the different fluxes are determined to ensure enough time for lithium-ion diffusion and intercalation in both electrolyte and cathode: $J_{1C} = 0.125\ \mathrm{Wm^{-2}}$, $J_{2C} = 0.25\ \mathrm{Wm^{-2}}$, $J_{6C} = 0.75\ \mathrm{Wm^{-2}}$, and $J_{8C} = 1\ \mathrm{Wm^{-2}}$ are used for the 1C, 2C, 6C, and 8C models, respectively,[38] and different fluxes result in different concentration gradients, i.e., Fick's first law is applied: $J = -D(\partial\phi/\partial y)$, where ϕ is lithium-ion concentration and D is diffusivity.

The Fluid Flow and Static Structural modules, and an Application Customization Toolkit (ACT) in ANSYS, are used to conduct computational simulations of fluid–solid interaction (FSI). That is, FSI is a transient extension that connects the computational fluid dynamics software tool, CFX, with the structural finite element analysis (FEA). FSI enables interpolating transient CFX results from the CFX mesh to the FEA mesh at each step of the analysis. Using a finite element information extension detailing nodes and element-related information at the mechanical interface, we then calculate the lithiation stage as follows: $\text{Lithiation stage} = \sum_i V_i \left(\frac{\sum_{j=1}^{j=10} \phi_j}{10} \right) \Big/ V_T$, where $i = 1$ to 57,456 for the number of elements, $j = 1$ to 10 for the 10-node tetrahedral element, V_i is the volume of each element, and V_T = the total volume of the electrode domain.

The electrolyte plays an important role in the performance of lithium-ion batteries. Generally, battery electrolytes are optimized for maximizing conductivity and electrochemical stability.[39,40] Ethylene carbonate (EC) is used as the electrolyte material in the finite element models because it has many beneficial properties such as high conductivity, high dipole moment (i.e., resulting in high ionic conductivity due to the dissociation of the lithium salt), yet high viscosity of electrolyte resulting in low fluidity (i.e., ionic movement). Since a commercial

Downloaded from https://www.cambridge.org/core. North Carolina State University, on 05 Oct 2017 at 13:29:53, subject to the Cambridge Core terms of use, available at https://www.cambridge.org/core/terms. https://doi.org/10.1557/jmr.2016.373

$LiFePO_4$ battery is a layered structure composed of a cathode strip and an anode strip with a separator between them,[32,41] one dimensional lithium-ion mass flux (J) along the y-axis is used as the driving force for the system (Fig. 1). As a result, lithium-ion concentration will vary continuously inside the half-cell system along the direction of lithium-ion mass flux. Different fluxes will result in different concentration gradients as Fick's first law is applied. In this study, it is assumed that the diffusion coefficient of electrolyte and the electrode are constant: $D_{\text{electrolyte}} = 1 \times 10^{-10}$ m^2/s,[42] and $D_{\text{LiFePO}_4} = D_{\text{FePO}_4} = 1 \times 10^{-15}$ m^2/s,[43] respectively. Thus, the lithium-ion concentration in the electrolyte changes more rapidly than that of the cathode. Hence, when the lithium-ion concentration in the electrolyte is 100%, only the surfaces of the particles will show 100% concentration (i.e., fully saturated) and the lithiation of the electrode is still in progress: the lithiation process in the cathode is then driven by Fick's second law: $\partial\phi/\partial t = -D\left(\partial^2\phi/\partial y^2\right)$.

The phase transformation in cathode materials is considered and the C-rate dependent volume misfits are adopted from the experimental observations.[44] Therefore, we incorporate volume misfits as follows: $\Delta V = 5.6\%$, 5.25%, 4.7%, and 4.5% for 1C, 2C, 6C, and 8C, respectively. Concentration-dependent anisotropic material properties for the cathode are also incorporated: the anisotropic material property matrix [C] is defined as $C(x) = x[C]^{\text{LiFePO}_4} + (1-x)[C]^{\text{FePO}_4}$, where x represents the fraction of lithium-rich phase ($0 \le x \le 1$). Orthorhombic elastic constants for both the lithium-rich and lithium-poor phases are obtained from Maxisch and Ceder (calculated from first principles)[45] (Table I). The shrinking-core model developed by Srinivasan and Newman[33] is adopted to simulate the first-order phase transformation. The lithium-rich phase will initially nucleate at the surface as such locations exhibit less interfacial area between the two phases[46] and the phase nucleation is along the shortest diffusion length (along the radial direction).[28,29,47] As a result, the phase boundary propagation wave along the radial direction is formed because of the relatively low energy barrier.

The concentration gradient profiles from the CFX of the analysis are imported into the FEA module via the ACT to calculate the corresponding mechanical responses of lithium-ion batteries at the cathode–electrolyte interface based on the stress–strain relation: $[\sigma] = [C]([\varepsilon] - \Delta V \Delta\phi)$. The stress fields on the interfaces with different volume fractions (i.e., particle sizes) at different lithiation stages and under different C-rates are investigated.

TABLE I. Material properties for cathodes and electrolytes.

	Parameter	Symbol	Value
EC [Ref. 40]	Density	ρ	1.321 g/cm^3
	Molar mass	M	88.06 g/mol
	Viscosity	η	1900 Pa s
$FePO_4$ [Ref. 45]	Young's modulus	E_X	133.15 GPa
		E_Y	121.12 GPa
		E_Z	101.68 GPa
	Shear modulus	G_{XY}	45.6 GPa
		G_{YZ}	32.5 GPa
		G_{XZ}	43 GPa
	Poisson's ratio	υ_{XY}	0.23
		υ_{YZ}	−0.02
		υ_{XZ}	0.45
	Elastic stiffness	C_{11}	137.4 GPa
		C_{22}	146.0 GPa
		C_{33}	132.0 GPa
		C_{44}	40.8 GPa
		C_{55}	38.2 GPa
		C_{66}	42.1 GPa
		C_{12}	41.0 GPa
		C_{13}	29.1 GPa
		C_{23}	29.1 GPa
$LiFePO_4$ [Ref. 45]	Young's modulus	E_X	98.41 GPa
		E_Y	157.3 GPa
		E_Z	146.3 GPa
	Shear modulus	G_{XY}	42.4 GPa
		G_{YZ}	34.9 GPa
		G_{XZ}	47.8 GPa
	Poisson's ratio	υ_{XY}	0.31
		υ_{YZ}	0.17
		υ_{XZ}	0.22
	Elastic stiffness	C_{11}	164.3 GPa
		C_{22}	162.9 GPa
		C_{33}	181.1 GPa
		C_{44}	40.8 GPa
		C_{55}	40.5 GPa
		C_{66}	43.9 GPa
		C_{12}	61.1 GPa
		C_{13}	54.9 GPa
		C_{23}	67.7 GPa
$FePO_4$ ↓ $LiFePO_4$ [Ref. 53]	Volume change	ΔV_X	0.058%
		ΔV_Y	0.045%
		ΔV_Z	−0.013%

III. RESULTS AND DISCUSSION

Several published studies have focused on the topic of the effect of mechanical stresses in lithium-ion batteries. Isolated cathodes, anodes, or electrolyte were generally considered in these studies, and as a result a fundamental knowledge of mechanical stresses at the cathode–electrolyte interface is not available in the literature. In this current work, we aim to identify how coupling factors (e.g., lithiation, C-rates, electrolyte, volume change, particle size, and phase transformation) relate to mechanical responses at the cathode–electrolyte interface.

Figure 2 provides contour plots of C-rate dependent lithiation in a half-cell system. (a)–(d) 1C and (e)–(h) 6C models are compared and normalized time to demonstrate the evolution of lithium-ion concentration. 100 nm-sized cathode particles are used. The concentration of electrolyte changes more rapidly than that of the cathode because the diffusivity of lithium ions in electrolyte is much higher than that in the solid electrode. The results

Downloaded from https://www.cambridge.org/core. North Carolina State University Libraries, on 01 Dec 2016 at 15:53:28, subject to the Cambridge Core terms of use, available at https://www.cambridge.org/core/terms. https://doi.org/10.1557/jmr.2016.373

indicate that though the lithium flux is induced at the same time at the inlet boundary (time = 0 as a rest condition) for both the 1C and 6C models, the electrode is fully saturated in a shorter time under a higher C-rate [Fig. 2(h)]. In the current study, we used 0% to present "initial" lithium-ion concentration, and it does not represent zero lithium-ion concentration in the electrolyte. Since a half-cell system is simulated and only electrolyte and cathode are included, any increases in lithium concentration in electrolyte and electrode are due to the decrease in lithium content in anode. In addition, our computational simulations have provided a visualized lithium-ion concentration distribution in the half-cell system, and these results are comparable to an analytical study by Guduru et al.[48] In the current work, our study limitation lies on the assumption of electrons can reach all the positions where Li^+ ion intercalation takes place, and therefore no polarization of the electrode occurs.[49,50] Thus, we have provided an ideal model that assuming no other resistance occurs (e.g., state of lithiation, current, rate of reaction etc.) at the electrode/electrolyte interface during the intercalation process. As a result, when electrolyte concentration reaches 100%, it is implied that electrolyte lithium-ion concentration is saturated, and therefore, lithium-ion concentration on the surface of the electrode particle is determined by the lithium-ion concentration in the electrolyte (Fig. 2). As shown in Fig. 3, the lithium-rich phase nucleates on the surface of the particle and the phase transformation occurs along the radial direction. The results demonstrate the phase transformation of the 1C model at different lithiation stages, where 100 nm-sized cathode particles are used (Fig. 3).

Diffusion-induced stress during (dis)charging of the half-cell system is investigated. At 50% lithiation, normal stresses on models with coupled effects from particle sizes (i.e., volume fraction) and C-rate are studied: Fig. 4(a) shows normal stress on the model with 60 nm particles under 1C-rate discharging, Fig. 4(b) shows normal stress on the model with 120 nm particles under 1C-rate discharging, and Fig. 4(c) shows normal stress on the model with 120 nm particles under 6C-rate discharging. The effect of particle size has been investigated in Figs. 4(a) and 4(b), suggesting that an increase in particle size (i.e., volume fraction) increases both compressive and tensile stresses in the half-cell system. As the particle size increases, the surface area of the cathode particles

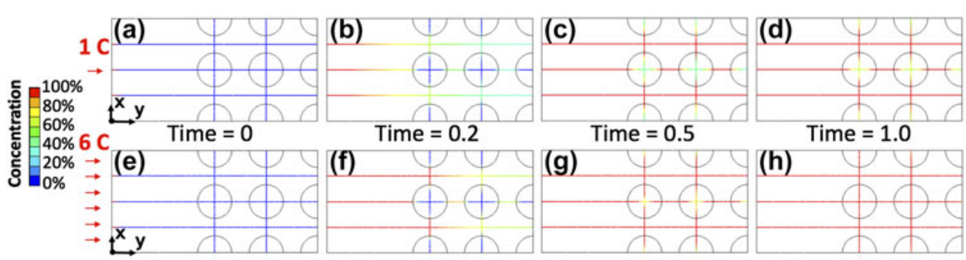

FIG. 2. Our results demonstrate our computational capability for simulating C-rate dependent lithiation. (a)–(d) 1C and (e)–(h) 6C models are compared and normalized time is used to demonstrate the evolution of lithium-ion concentration. 100 nm-sized cathode particles are used. The results indicate that although lithium flux is induced at the same time at the inlet boundary, the electrode is fully saturated in a shorter time under a higher C-rate.

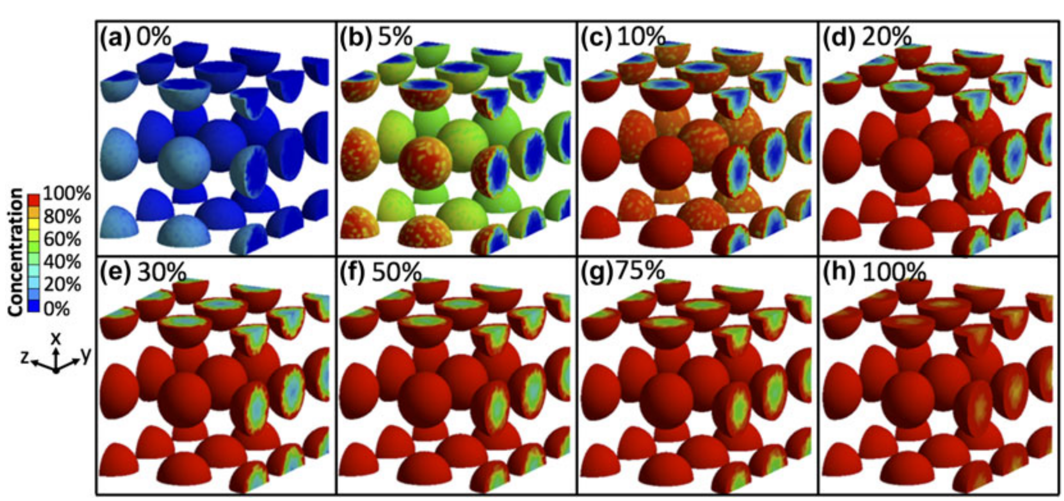

FIG. 3. Our results demonstrate our computational capability for simulating phase transformation in core–shell cathode 100 nm-sized particles. The model shows phase transformation in the cathode at different lithiation stages: (a) 0%, (b) 5%, (c) 10%, (d) 20%, (e) 30%, (f) 50%, (g) 75%, and (h) 100% for the 1C-rate model.

Downloaded from https://www.cambridge.org/core. North Carolina State University, on 05 Oct 2017 at 13:09:53, subject to the Cambridge Core terms of use, available at https://www.cambridge.org/core/terms. https://doi.org/10.1557/jmr.2016.373

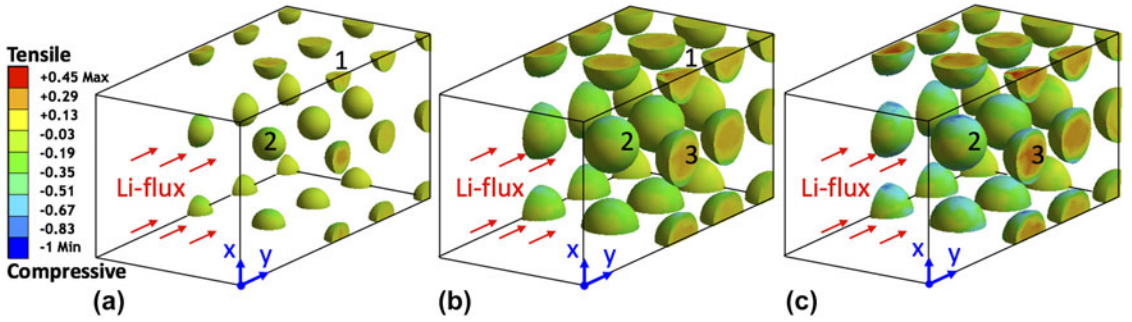

FIG. 4. The effects of particle size and C-rate have been investigated at 50% lithiation. (a) 60 nm versus (b) 120 nm models: the contour plots of mechanical stresses show that doubling the particle size increases both compressive and tensile stresses in the half-cell system, and the changes in compression (1.82 times greater; denoted at position 2) during lithiation is higher than that in tension (1.42 times greater; denoted at position 1). (b) 1C versus (c) 6C models: The C-rate six times higher causes a 1.57 times greater tensile stress (denoted at position 3) and 1.64 times greater compressive stress (denoted at position 2). Both compressive and tensile stresses are strongly affected by C-rate, due to the surface concentration gradient being higher with higher C-rate.

also increases, resulting in larger available lithium intercalation areas. It is observed that the larger particle size (i.e., 60 nm versus 120 nm) causes 1.40 times greater tensile stress [denoted at position "1" in Figs. 4(a)–4(b)] and 1.82 times greater compressive stress [denoted at position "2" in Figs. 4(a)–4(b)]. We conclude that compressive stress on the surface of a particle is strongly affected by the particle size. In the current study, the phase transformation is considered during the lithiation (as observed in experiments), different sizes of spherical particle would have different anisotropic material properties involved during the phase transformation attributed to diffusion-induced stresses. Thus, in this case, while comparing Fig. 4(a) versus 4(b) when the ion flux density is kept the same for two different particles (60 nm versus 120 nm), it does not imply that C-rate is instead being compared. The effect of C-rate is investigated (1C versus 6C) in Figs. 4(b) and 4(c). The C-rate that was six times larger causes 1.57 times greater tensile stress [denoted at position "3" in Figs. 4(b)–4(c)] and 1.64 times greater compressive stress [denoted at position "2" in Figs. 4(b)–4(c)]. Both compressive stress and tensile stress are strongly affected by the C-rate, which is due to the surface concentration gradient being higher with higher C-rate. Studies have reported that the tensile stress is observed in the center of the electrode while compressive stress is observed on the surface of the electrode.[37] Moreover, higher stresses occurring at the forefront of particles have been observed in most cases, suggesting that there is a need to relieve stresses at the electrode–electrolyte interface. Nevertheless, it is still unable to claim that these stresses are reasons for mechanical degradation in lithium-ion batteries. As Dr. Nancy Dudney has pointed out,[51] mechanical failure should not be a concern for intercalation-type cathodes, since the volume change upon cycling is only 2–7%, much smaller than that in alloying-type anodes which is typically 100%. Moreover, Christensen and Newman[23]

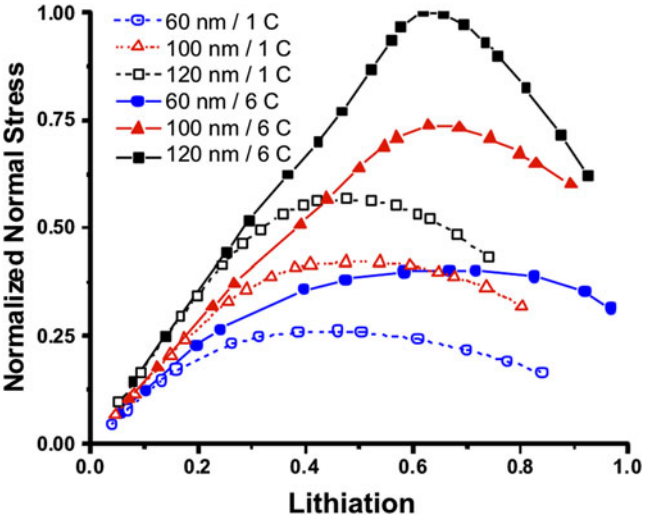

FIG. 5. Effect of particle size and C-rate on normalized normal stress at the electrolyte–electrode interface during lithiation. It is observed that mechanical stresses initially increase to overcome energy barriers in the two-phase region (i.e., between the lithium-rich phase and the lithium-poor phase) and the stresses are relieved afterward. As C-rate increases, the peak mechanical stress occurs when the cathode is more lithiated and related to the lithium-ion concentration gradient inside the half-cell system.

have showed that a compressive external stress could reduce the likelihood of particle fracture because the fracture threshold for the tensile stress is typically much lower than that for the compressive stress.

Figure 5 summarizes the effect of C-rate and particle size on normalized stresses at the electrolyte–electrode interface during lithiation. The results suggest that higher C-rate causes higher stresses. Moreover, it is observed that the stress initially increases to overcome energy barriers in the two-phase region (i.e., lithium-rich phase and lithium-poor phase) and the stress is relieved afterward. This phenomenon is also observed in other battery chemistries such as $LiCoO_2$ (Ref. 52) and $LiMn_2O_4$ (Ref. 24). Interestingly, as C-rate increases, the peak

Downloaded from https://www.cambridge.org/core. North Carolina State University Libraries, on 01 Dec 2016 at 15:53:28, subject to the Cambridge Core terms of use, available at https://www.cambridge.org/core/terms. https://doi.org/10.1557/jmr.2016.373

stress occurs when the cathode is more lithiated.[37] The lithium concentration gradient also increases as a result and mechanical stress is more prominent when the concentration gradient increases. The results also suggest that normal stress increases with larger particle size (i.e., volume fraction). Increasing the particle size yields increases in the available lithiation surface area. Since larger particle sizes and higher C-rates result in higher stresses, battery degradation would be expected in these conditions. Simulation results confirm that there are relationships between mechanical stresses and many design parameters for lithium-ion batteries.

IV. CONCLUSIONS

Current study considers factors such as electrolyte, C-rate, C-rate dependent volume changes, cathode particle sizes (i.e., volume fractions), and the phase transformation of the electrodes to better understand electrochemical and mechanical relationships in lithium-ion batteries. The coupled domains of electrolyte and the cathode particles are modeled in a half-cell system to investigate the evolution of mechanical stress during lithium-ion battery discharging. The finite element models have been developed using Fluid Flow and Static Structural modules in ANSYS Workbench. A FSI module connecting the computational fluid dynamics with the structural FEA is included.

The results indicate that although lithium flux is induced at the inlet boundary at the same time for different C-rate models, the electrode is fully saturated in a shorter time under higher C-rates. The lithium-rich phase nucleates on the surface of the particle and the phase transformation occurs along the radial direction. The results show that under higher C-rate with larger available lithium intercalation areas (i.e., larger particles), mechanical stresses increase more dramatically in compression, suggesting that compressive stress is a much more critical factor for diffusion-induced stresses in lithium-ion batteries. The methods and findings could also be broadly applicable to other battery technologies, such as sodium-ion, magnesium-ion, and potassium-ion. The current study suggests that integrating electrolyte/electrode material selections into battery manufacturing could potentially increase battery performance, as well as provide higher power and greater energy densities in many applications.

REFERENCES

1. Y-M. Chiang: Building a better battery. *Science* **330**, 1485 (2010).
2. B. Kang and G. Ceder: Battery materials for ultrafast charging and discharging. *Nature* **458**, 190 (2009).
3. D. Aurbach, B. Markovsky, G. Salitra, E. Markevich, Y. Talyossef, M. Koltypin, L. Nazar, B. Ellis, and D. Kovacheva: Review on electrode–electrolyte solution interactions, related to cathode materials for Li-ion batteries. In *IBA—HBC 2006 Selected Papers from the International Battery Association & Hawaii Battery Conference 2006*, Vol. **165**, Waikoloa, Hawaii, USA, 2007; p. 491.
4. D. Aurbach, Y. Talyosef, B. Markovsky, E. Markevich, E. Zinigrad, L. Asraf, J.S. Gnanaraj, and H.J. Kim: Design of electrolyte solutions for Li and Li-ion batteries: A review. *Electrochim. Acta* **50**, 247 (2004).
5. H. Ju, J. Wu, and Y.H. Xu: Revisiting the electrochemical impedance behaviour of the $LiFePO_4$/C cathode. *J. Chem. Sci.* **125**, 687 (2013).
6. F.C. Strobridge, B. Orvananos, M. Croft, H.C. Yu, R. Robert, H. Liu, Z. Zhong, T. Connolley, M. Drakopoulos, K. Thornton, and C.P. Grey: Mapping the inhomogeneous electrochemical reaction through porous $LiFePO_4$-electrodes in a standard coin cell battery. *Chem. Mater.* **27**, 2374 (2015).
7. R. Deshpande, Y.T. Cheng, M.W. Verbrugge, and A. Timmons: Diffusion induced stresses and strain energy in a phase-transforming spherical electrode particle. *J. Electrochem. Soc.* **158**, A718 (2011).
8. C.K. ChiuHuang and H.Y.S. Huang: Stress evolution on the phase boundary in $LiFePO_4$ particles. *J. Electrochem. Soc.* **160**, A2184 (2013).
9. M. Stamps, J.W. Eischen, and H.-Y.S. Huang: Particle- and Crack-Size Dependency of Lithium-ion Battery Materials $LiFePO_4$. *AIMS Mater. Sci*. **3**(1), 190 (2016).
10. H.-Y.S. Huang and Y.-X. Wang: Dislocation Based Stress Developments in Lithium-Ion Batteries. *J. Electrochem. Soc.* **159**(6), A815 (2012).
11. Y-T. Cheng and M.W. Verbrugge: Diffusion-induced stress, interfacial charge transfer, and criteria for avoiding crack initiation of electrode particles. *J. Electrochem. Soc.* **157**, A508 (2010).
12. Y.T. Cheng and M.W. Verbrugge: The influence of surface mechanics on diffusion induced stresses within spherical nanoparticles. *J. Appl. Phys.* **104**, 083521 (2008).
13. Y.T. Cheng and M.W. Verbrugge: Evolution of stress within a spherical insertion electrode particle under potentiostatic and galvanostatic operation. *J. Power Sources* **190**, 453 (2009).
14. R. Deshpande, Y.T. Cheng, and M.W. Verbrugge: Modeling diffusion-induced stress in nanowire electrode structures. *J. Power Sources* **195**, 5081 (2010).
15. R. Deshpande, Y. Qi, and Y.T. Cheng: Effects of concentration-dependent elastic modulus on diffusion-induced stresses for battery applications. *J. Electrochem. Soc.* **157**, A967 (2010).
16. R. Deshpande, M. Verbrugge, Y.T. Cheng, J. Wang, and P. Liu: Battery cycle life prediction with coupled chemical degradation and fatigue mechanics. *J. Electrochem. Soc.* **159**, A1730 (2012).
17. J. Park, W. Lu, and A.M. Sastry: Numerical simulation of stress evolution in lithium manganese dioxide particles due to coupled phase transition and intercalation. *J. Electrochem. Soc.* **158**, A201 (2011).
18. M. Park, X. Zhang, M. Chung, G.B. Less, and A.M. Sastry: A review of conduction phenomena in Li-ion batteries. *J. Power Sources* **195**, 7904 (2010).
19. X. Zhang, A.M. Sastry, and W. Shyy: Intercalation-induced stress and heat generation within single lithium-ion battery cathode particles. *J. Electrochem. Soc.* **155**, A542 (2008).
20. X. Zhang, W. Shyy, and A.M. Sastry: Numerical simulation of intercalation-induced stress in Li-ion battery electrode particles. *J. Electrochem. Soc.* **154**, A910 (2007).
21. Z. Zhang: *High Voltage Electrolyte for Lithium Batteries* (Argonne National Laboratory Presentation, Washington, DC, 2012).
22. J. Christensen and J. Newman: A mathematical model of stress generation and fracture in lithium manganese oxide. *J. Electrochem. Soc.* **153**, A1019 (2006).

Downloaded from https://www.cambridge.org/core. North Carolina State University, on 05 Oct 2017 at 13:12:53, subject to the Cambridge Core terms of use, available at https://www.cambridge.org/core/terms. https://doi.org/10.1557/jmr.2016.373

23. J. Christensen and J. Newman: Stress generation and fracture in lithium insertion materials. *J. Solid State Electrochem.* **10**, 293 (2006).
24. M. Zhu, J. Park, and A.M. Sastry: Fracture analysis of the cathode in Li-ion batteries: A simulation study. *J. Electrochem. Soc.* **159**, A492 (2012).
25. S. Renganathan, G. Sikha, S. Santhanagopalan, and R. E. White: Theoretical analysis of stresses in a lithium ion cell. *J. Electrochem. Soc.* **157**, A155 (2010).
26. S. Renganathan and R.E. White: Semianalytical method of solution for solid phase diffusion in lithium ion battery electrodes: Variable diffusion coefficient. *J. Power Sources* **196**, 442 (2011).
27. G. Chen, X. Song, and T.J. Richardson: Electron microscopy study of the $LiFePO_4$ to $FePO_4$ phase transition. *Electrochem. Solid-State Lett.* **9**, A295 (2006).
28. S-i. Nishimura, G. Kobayashi, K. Ohoyama, R. Kanno, M. Yashima, and A. Yamada: Experimental visualization of lithium diffusion in Li_xFePO_4. *Nat. Mater.* **7**, 707 (2008).
29. A. Yamada, H. Koizumi, S-i. Nishimura, N. Sonoyama, R. Kanno, M. Yonemura, T. Nakamura, and Y. Kobayashi: Room-temperature miscibility gap in Li_xFePO_4. *Nat. Mater.* **5**, 360 (2006).
30. A. Yamada, H. Koizumi, N. Sonoyama, and R. Kanno: Phase change in Li_xFePO_4. *Electrochem. Solid-State Lett.* **8**, A409 (2005).
31. C-K. ChiuHuang and H-Y.S. Huang: A diffusion model in a two-phase interfacial zone for nanoscale lithium-ion battery materials. In *Proceedings of the ASME International Mechanical Engineering Congress and Exposition* (ASME International, Houston, 2012); p. 1231.
32. C-K. ChiuHuang, C. Zhou, and H-Y. Shadow Huang: In situ imaging of lithium-ion batteries via the secondary ion mass spectrometry. *J. Nanotechnol. Eng. Med.* **5**, 021002 (2014).
33. V. Srinivasan and J. Newman: Discharge model for the lithium iron-phosphate electrode. *J. Electrochem. Soc.* **151**, A1517 (2004).
34. C.K. ChiuHuang and H-Y.S. Huang: Critical lithiation for C-rate dependent mechanical stresses in $LiFePO_4$. *J. Solid State Electrochem.* **19**, 2245 (2015).
35. F. Sauvage, E. Baudrin, M. Morcrette, and J.M. Tarascon: Pulsed laser deposition and electrochemical properties of $LiFePO_4$ thin films. *Electrochem. Solid-State Lett.* **7**, A15 (2004).
36. G. Brunetti, D. Robert, P. Bayle-Guillemaud, J.L. Rouviere, E.F. Rauch, J.F. Martin, J.F. Colin, F. Bertin, and C. Cayron: Confirmation of the Domino-Cascade model by $LiFePO_4/FePO_4$ precession electron diffraction. *Chem. Mater.* **23**, 4515 (2011).
37. J. Christensen: Modeling diffusion-induced stress in Li-ion cells with porous electrodes. *J. Electrochem. Soc.* **157**, A366 (2010).
38. Y.Y. Li, F. El Gabaly, T.R. Ferguson, R.B. Smith, N.C. Bartelt, J.D. Sugar, K.R. Fenton, D.A. Cogswell, A.L.D. Kilcoyne, T. Tyliszczak, M.Z. Bazant, and W.C. Chueh: Current-induced transition from particle-by-particle to concurrent intercalation in phase-separating battery electrodes. *Nat. Mater.* **13**, 1149 (2014).
39. L.O. Valoen and J.N. Reimers: Transport properties of $LiPF_6$-based Li-ion battery electrolytes. *J. Electrochem. Soc.* **152**, A882 (2005).
40. G.A. Nazri and G. Pistoia, eds.: *Lithium Batteries: Science and Technologies* (Springer, New York, 2009); pp. 509–529.
41. S.C. Nagpure, R.G. Downing, B. Bhushan, S.S. Babu, and L. Cao: Neutron depth profiling technique for studying aging in Li-ion batteries. *Electrochim. Acta* **56**, 4735 (2011).
42. K. Hayamizu: Temperature dependence of self-diffusion coefficients of ions and solvents in ethylene carbonate, propylene carbonate, and diethyl carbonate single solutions and ethylene carbonate plus diethyl carbonate binary solutions of LiPF6 studied by NMR. *J. Chem. Eng. Data* **57**, 2012 (2012).
43. A.V. Churikov, A.V. Ivanishchev, I.A. Ivanishcheva, V.O. Sycheva, N.R. Khasanova, and E.V. Antipov: Determination of lithium diffusion coefficient in $LiFePO_4$ electrode by galvanostatic and potentiostatic intermittent titration techniques. *Electrochim. Acta* **55**, 2939 (2010).
44. Q. Liu, H. He, Z.F. Li, Y.D. Liu, Y. Ren, W.Q. Lu, J. Lu, E.A. Stach, and J. Xie: Rate-dependent, Li-ion insertion/deinsertion behavior of $LiFePO_4$ cathodes in commercial 18650 $LiFePO_4$ cells. *ACS Appl. Mater. Interfaces* **6**, 3282 (2014).
45. T. Maxisch and G. Ceder: Elastic properties of olivine Li_xFePO_4 from first principles. *Phys. Rev. B: Condens. Matter Mater. Phys.* **73**, 174112 (2006).
46. M. Tang, J.F. Belak, and M.R. Dorr: Anisotropic phase boundary morphology in nanoscale olivine electrode particles. *J. Phys. Chem. C* **115**, 4922 (2011).
47. L. Laffont, C. Delacourt, P. Gibot, M.Y. Wu, P. Kooyman, C. Masquelier, and J.M. Tarascon: Study of the $LiFePO_4/FePO_4$ two-phase system by high-resolution electron energy loss spectroscopy. *Chem. Mater.* **18**, 5520 (2006).
48. A. Guduru, P.W.C. Northrop, S. Jain, A.C. Crothers, T.R. Marchant, and V.R. Subramanian: Analytical solution for electrolyte concentration distribution in lithium-ion batteries. *J. Appl. Electrochem.* **42**, 189 (2012).
49. Y.G. Wang, Y.R. Wang, E.J. Hosono, K.X. Wang, and H.S. Zhou: The design of a $LiFePO_4$/carbon nanocomposite with a core-shell structure and its synthesis by an in situ polymerization restriction method. *Angew. Chem., Int. Ed.* **47**, 7461 (2008).
50. X.D. Zhang, Y.K. Hou, W. He, G.H. Yang, J.J. Cui, S.K. Liu, X. Song, and Z. Huang: Fabricating high performance lithium-ion batteries using bionanotechnology. *Nanoscale* **7**, 3356 (2015).
51. J.C. Li, Q.L. Zhang, X.C. Xiao, Y.T. Cheng, C.D. Liang, and N.J. Dudney: Unravelling the impact of reaction paths on mechanical degradation of intercalation cathodes for lithium-ion batteries. *J. Am. Chem. Soc.* **137**, 13732 (2015).
52. C. Lim, B. Yan, L.L. Yin, and L.K. Zhu: Simulation of diffusion-induced stress using reconstructed electrodes particle structures generated by micro/nano-CT. *Electrochim. Acta* **75**, 279 (2012).
53. G. Kobayashi, S.I. Nishimura, M.S. Park, R. Kanno, M. Yashima, T. Ida, and A. Yamada: Isolation of solid solution phases in size-controlled Li_xFePO_4 at room temperature. *Adv. Funct. Mater.* **19**, 395 (2009).

Downloaded from https://www.cambridge.org/core. North Carolina State University Libraries, on 01 Dec 2016 at 15:53:28, subject to the Cambridge Core terms of use, available at https://www.cambridge.org/core/terms. https://doi.org/10.1557/jmr.2016.373